More humid interglacials in Ecuador during the past 500 kyr linked to latitudinal shifts of the equatorial front and the Intertropical Convergence Zone in the eastern tropical Pacific

Daniel Rincón-Martínez,[1] Frank Lamy,[1] Sergio Contreras,[2] Guillaume Leduc,[3] Edouard Bard,[4] Cornelia Saukel,[1] Thomas Blanz,[3] Andreas Mackensen,[1] and Ralf Tiedemann[1]

Received 8 October 2009; revised 10 February 2010; accepted 24 March 2010; published 2 June 2010.

[1] Studying past changes in the eastern equatorial Pacific Ocean dynamics and their impact on precipitation on land gives us insight into how the Intertropical Convergence Zone (ITCZ) movements and the El Niño-Southern Oscillation modulate regional and global climate. In this study we present a multiproxy record of terrigenous input from marine sediments collected off the Ecuadorian coast spanning the last 500 kyr. In parallel we estimate sea surface temperatures (SST) derived from alkenone paleothermometry for the sediments off the Ecuadorian coast and complement them with alkenone-based SST data from the Panama Basin to the north in order to investigate SST gradients across the equatorial front. Near the equator, today's river runoff is tightly linked to SST, reaching its maximum either during the austral summer when the ITCZ migrates southward or during El Niño events. Our multiproxy reconstruction of riverine runoff indicates that interglacial periods experienced more humid conditions than the glacial periods. The north-south SST gradient is systematically steeper during glacial times, suggesting a mean background climatic state with a vigorous oceanic cold tongue, resembling modern La Niña conditions. This enhanced north-south SST gradient would also imply a glacial northward shift of the Intertropical Convergence Zone at least in vicinity of the cold tongue: a pattern that has not yet been reproduced in climate models.

Citation: Rincón-Martínez, D., F. Lamy, S. Contreras, G. Leduc, E. Bard, C. Saukel, T. Blanz, A. Mackensen, and R. Tiedemann (2010), More humid interglacials in Ecuador during the past 500 kyr linked to latitudinal shifts of the equatorial front and the Intertropical Convergence Zone in the eastern tropical Pacific, *Paleoceanography*, *25*, PA2210, doi:10.1029/2009PA001868.

1. Introduction

[2] Today the average state of the eastern equatorial Pacific (EEP) is characterized by a pronounced north-south sea surface temperature (SST) gradient, with warm and stratified waters remaining north of the equator (Eastern Pacific Warm Pool (EPWP)), while a cold tongue, associated with equatorial upwelling and advection of cold waters from the Peru Current, is located south of the equator. On interannual to decadal timescales these conditions are significantly modified through atmosphere-ocean changes related to El Niño-Southern Oscillation (ENSO) dynamics. During the warm (El Niño) phase of ENSO, warm waters spread eastward from the western Pacific warm pool, and SSTs in the cold tongue are substantially warm. Conversely, during the cold (La Niña) phase, the cold tongue strengthens, and the cross-equatorial SST gradient in the EEP is substantially larger [*McPhaden et al.*, 2006; *Wang and Fiedler*, 2006].

[3] Long-term ENSO changes on millennial, orbital, or even tectonic timescales throughout the Plio-Pleistocene and their role for global climate have been intensively discussed [*Markgraf and Diaz*, 2000; *Cane*, 2004; *Fedorov et al.*, 2006]. On glacial-interglacial timescales, some authors suggest that the average glacial state of the EEP was more similar to that occurring during modern El Niño years [*Koutavas et al.*, 2002; *Koutavas and Lynch-Stieglitz*, 2003], while others consider a mean glacial state similar to the cold La Niña phase [*Andreasen and Ravelo*, 1997; *Andreasen et al.*, 2001; *Martínez et al.*, 2003]. Low-latitude orbital forcing has been suggested to exert control on the mean state of ENSO as well [*Clement et al.*, 1999; *Pena et al.*, 2008]. Other authors again link SST changes in the EEP to high-latitude climate variability in the Southern Hemisphere without invoking ENSO changes [*Pisias and Mix*, 1997; *Lea et al.*, 2000; *Feldberg and Mix*, 2003; *Spero et al.*, 2003; *Lea et al.*, 2006].

[4] Hence, the scenarios drawn from these studies are diverse. Most studies focus on paleoceanographic features such as SST, paleoproductivity, or water stratification, whereas continental climate changes are rarely considered [e.g., *Pahnke et al.*, 2007]. Yet, modern atmosphere-ocean reorganizations

[1]Alfred Wegener Institute for Polar and Marine Research, Bremerhaven, Germany.
[2]Max Planck Institute for Marine Microbiology, Bremen, Germany.
[3]Institut für Geowissenschaften, Christian Albrecht Universität, Kiel, Germany.
[4]CEREGE, Aix-Marseille Université, CNRS, Collège de France, IRD, Europôle Méditerranéen de L'Arbois, Aix-en-Provence, France.

0883-8305/10/2009PA001868

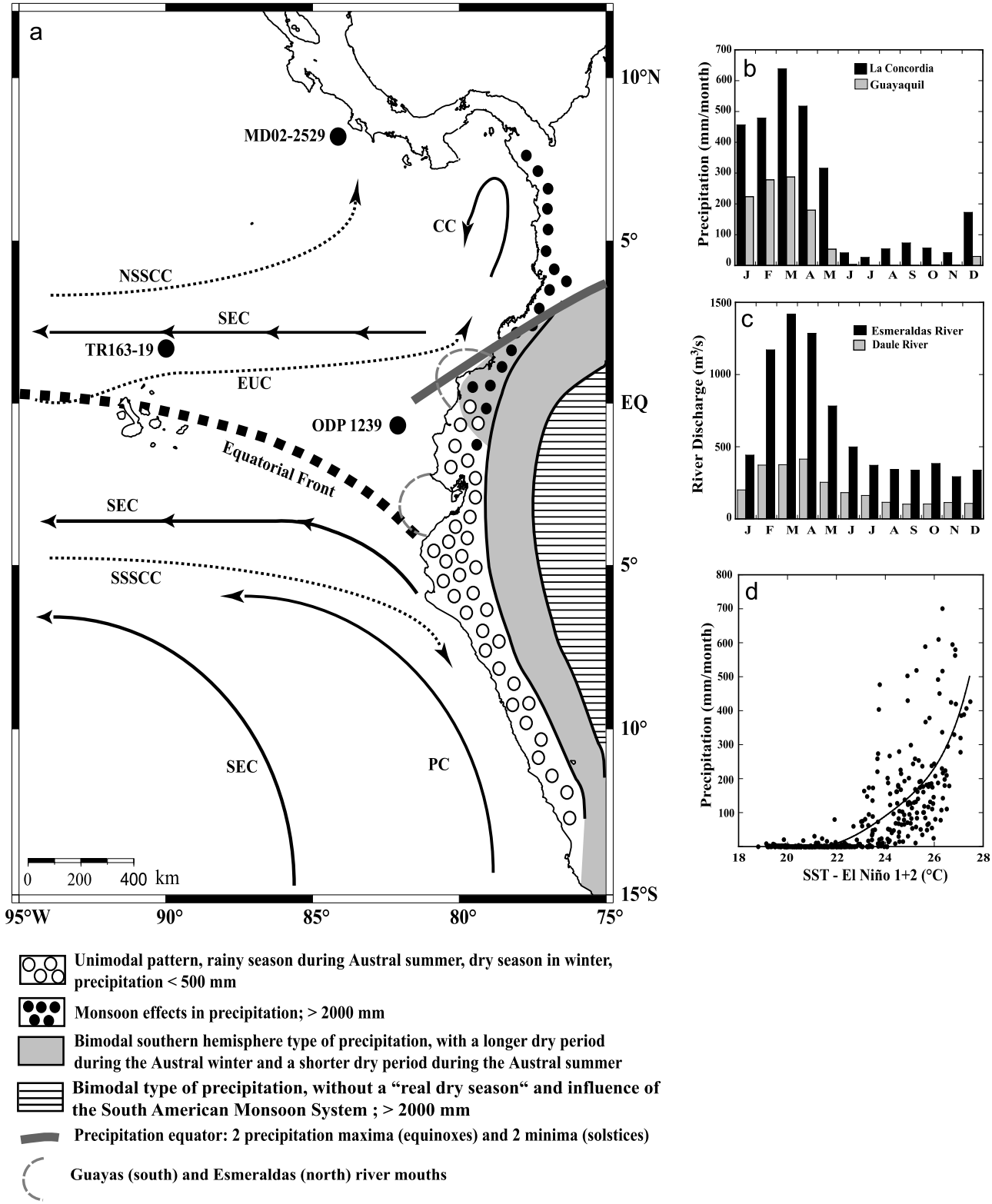
a
10°N
5°
EQ
5°
10°
15°S
95°W
90°
85°
80°
75°
MD02-2529
CC
NSSCC
SEC
TR163-19
EUC
ODP 1239
Equatorial Front
SEC
SSSCC
SEC
PC
0 200 400 km
b
La Concordia
Guayaquil
Precipitation (mm/month)
J F M A M J J A S O N D
c
Esmeraldas River
Daule River
River Discharge (m3/s)
J F M A M J J A S O N D
d
Precipitation (mm/month)
SST - El Niño 1+2 (°C)
Unimodal pattern, rainy season during Austral summer, dry season in winter, precipitation < 500 mm
Monsoon effects in precipitation; > 2000 mm
Bimodal southern hemisphere type of precipitation, with a longer dry period during the Austral winter and a shorter dry period during the Austral summer
Bimodal type of precipitation, without a "real dry season" and influence of the South American Monsoon System ; > 2000 mm
Precipitation equator: 2 precipitation maxima (equinoxes) and 2 minima (solstices)
Guayas (south) and Esmeraldas (north) river mouths

Figure 1

related to ENSO strongly impact onshore precipitation, particularly in northern Peru and coastal Ecuador. During El Niño phases, unusually warm EEP waters promote convection of the overlying atmosphere, while the Intertropical Convergence Zone (ITCZ) and associated precipitation anomalies shift farther south than during the regular seasonal cycle [*Horel and Cornejo-Garrido*, 1986; *Bendix*, 2000; *Bendix and Bendix*, 2006].

[5] Here, we present a combined analysis of proxy data that allude to paleoceanographic changes in the EEP and concomitant continental paleoclimate variations onshore during the past 500 kyr. The proxy profiles are derived from samples obtained from sediment cores off the coast of Ecuador and in the Panama Basin. A systematic pattern of changes in the terrigenous sediment input during glacial-interglacial periods can be linked to tropical rainfall changes over coastal Ecuador. These glacial-interglacial rainfall changes are paralleled by latitudinal shifts of the equatorial front (EF) moving southward during interglacials as is indicated by higher SST, enhanced surface water stratification, higher abundances of the foraminifera species *Globorotalia cultrata* relative to *Neogloboquadrina dutertrei*, and increases in mangrove biomarker accumulation rates. A comparison of our SST record with the EPWP SST record from Site MD02-2529 covering the past ~300 kyr indicates that fluctuations in the latitudinal SST gradients during glacial-interglacial periods across the EF in the EEP played a pivotal role in past precipitation changes in the region.

2. Modern Climatology and Oceanography at Studied Sites

[6] Our study is based on two sites in the EEP (Figure 1), the first of which is Ocean Drilling Program (ODP) Site 1239 (0°40.32′S, 82°4.86′W, 1414 m water depth) located at the northern margin of the eastern Pacific cold tongue close to the EF and ~120 km off the Ecuadorian coast. The area is characterized by a thermocline shoaling and local wind-driven upwelling that supplies nutrient-rich waters from the Equatorial Undercurrent (EUC) to the surface, creating highstanding stocks of phytoplankton and enhanced primary productivity rates [*Lukas*, 1986; *Fiedler et al.*, 1991; *Pennington et al.*, 2006]. The second site, MD02-2529 (08° 12.33′N, 84°07.32′W, 1619 m water depth), is situated close to the Costa Rica margin of the Panama Basin within the EPWP, where SSTs are above 27°C and sea surface salinities are below 33.2 practical salinity unit (psu) throughout the year [*Leduc et al.*, 2007].

2.1. EEP Oceanography

[7] A striking feature of the west coast of South America is the presence of unusually cool and highly saline ($T < 25$°C, $S > 34$ psu) surface waters extending westward slightly south of the equator. This cold tongue is fed by seasonal advection of cold waters from the Peru Current (PC) and by equatorial upwelling [*Pak and Zaneveld*, 1974; *Fiedler and Talley*, 2006]. The cold tongue is bounded by the EF, a narrow band located around the equator between the Peruvian coast and the Galapagos Islands (Figure 1). North of the EF, warm, low-salinity waters ($T < 25$°C, $S > 34$ psu) of the Panama Basin occur because of a large net heat flux, weak wind mixing, and intense rainfall beneath the ITCZ [*Pak and Zaneveld*, 1974; *Fiedler and Talley*, 2006].

[8] The cold tongue and associated frontal zone are persistent features, but their strength varies both seasonally and interannually. During austral winter, solar heating reinforces the meridional SST gradient, strengthening the southeasterly trade winds and the equatorial cold tongue and shifting the EF to its northernmost position. From January to April, SST increases south of the equator because of the subsidence of the southeast trades, resulting in a diffused southern position of the EF [*Pak and Zaneveld*, 1974; *Raymond et al.*, 2004; *de Szoeke et al.*, 2007]. The quasiperiodic El Niño-Southern Oscillation (ENSO) dominates the interannual variability in this region. The El Niño warm phase is related to anomalous eastward advection of warm water in the eastern Pacific cold tongue, associated with a weaker EF [*Pak and Zaneveld*, 1974; *Kessler*, 2006; *McPhaden et al.*, 2006; *Wang and Fiedler*, 2006]. At this time, variations in the water transports of the South Equatorial Current (SEC) and EUC induce a deepening of the thermocline, causing positive SST anomalies [*Kessler*, 2006]. The opposite conditions occur during the cool La Niña phase.

2.2. EEP Atmospheric Circulation

[9] The EEP atmospheric convection and its associated continental precipitation are mostly linked to the ITCZ and occur preferentially over the EPWP waters. This pattern is maintained most of the year by several positive feedbacks. First, the temperature asymmetry along the equator reinforces

Figure 1. (a) Schematic (sub)surface circulation in the eastern equatorial Pacific (modified after *Kessler* [2006]). Locations of ODP Site 1239, Site TR163-19, Site MD02-2529, and the Guayas and Esmeraldas river mouths and precipitation patterns over northern South America (modified after *Bendix and Lauer* [1992]). Upper layer currents (black arrows) are the SEC, South Equatorial Current; CC, Colombia Current; and PC, Peru or Humboldt Current. Subsurface currents (dashed arrows) are NSSCC, Northern Subsurface Countercurrent; SSSCC, Southern Subsurface Countercurrent; and EUC, Equatorial Undercurrent. (b) Mean monthly precipitation at Guayaquil (2.20°S, 79.90°W, 6 m above sea level (asl); Guayas Basin) and La Concordia (0.1°N, 79.30°W, 300 m asl; Esmeraldas Basin) metereological stations. (c) Mean monthly fluvial discharge of the Daule River (1.69°S, 79.99°W, 20 m asl; at La Capilla hydrological station), one of the main tributaries of the Guayas River, and the Esmeraldas River (0.52°N, 79.41°W, 50 m asl; at Esmeraldas hydrological station). (d) Polynomial fit between monthly SST at El Niño 1 + 2 region (0°S–10°S, 90°W–80°W) and monthly precipitation at Guayaquil meteorological station. SST data are generated from the World Ocean Atlas database [*Conkright et al.*, 2002]; precipitation [*Peterson and Russell*, 1997] and river discharges are from R-HydroNET (available at http://www.r-hydronet.sr.unh.edu/).

surface winds over the cold tongue, which further cools the water through evaporation and upwelling [*Xie and Philander*, 1994; *Xie*, 2004]. Second, the combination of cold surface waters with warm, dry air aloft results in large and persistent subtropical stratocumulus decks, which reflect much of the incoming solar radiation and help to maintain the cool SST of the "cold tongue" [*Klein and Hartmann*, 1993; *Raymond et al.*, 2004]. In addition, the northwest-southeast orientation of the coastline of South America combined with the topographic barrier of the Andes constrains winds to blow along the Peruvian coastline and induces coastal upwelling there [*Philander et al.*, 1996; *Xie*, 2004].

[10] During late austral summer, the north-south SST contrast is relaxed, the EF is weakest, and the ITCZ and associated precipitation migrate southward along the Colombian and Ecuadorian coasts [*Horel and Cornejo-Garrido*, 1986; *Bendix and Lauer*, 1992; *Hastenrath*, 2002; *Amador et al.*, 2006; *Poveda et al.*, 2006]. Conversely, a northward displacement of the ITCZ occurs during late austral winter, when the cold tongue is intensified and the advection of the Peru-Chile current is strongest [*Hastenrath*, 2002; *Amador et al.*, 2006; *Poveda et al.*, 2006; *de Szoeke et al.*, 2007].

[11] During an El Niño event the trade winds weaken along the equator, as atmospheric pressure rises in the western Pacific and falls in the eastern Pacific, and permit an eastward expansion of warm waters from the central Pacific [*McPhaden et al.*, 2006; *Wang and Fiedler*, 2006]. This phenomenon acts to weaken the Humboldt Current and the equatorial and coastal upwelling systems. Atmospheric convection cells and the associated precipitation of the ITCZ shift to the south, causing heavy rainfall over the northern Peruvian desert and coastal Ecuador [*Horel and Cornejo-Garrido*, 1986; *Neill and Jørgensen*, 1999; *Hastenrath*, 2002; *Waylen and Poveda*, 2002; *Poveda et al.*, 2006].

2.3. Guayas and Esmeraldas Drainage Systems, Precipitation, and Fluvial Runoff

[12] The Guayas and the Esmeraldas basins are the largest drainage systems in western Ecuador, both in terms of area (32,674 km^2 and 21,418 km^2, respectively) and water volume drained per area unit. Annual precipitation and river discharges in both basins, including the Coastal Mountain Range and the western slopes of the Andes at altitudes <1800 m above sea level, experience a unimodal pattern that is characterized by a rainy season from December to April. Precipitation and river runoff maxima occur in March and broadly coincide with the southernmost seasonal excursion of the ITCZ in the EEP and with the seasonal SST maximum at ODP Site 1239 (Figures 1b–1d). The rest of the year, precipitation is limited by the combined effects of low SST, atmospheric subsidence of dry air, and reduced insolation due to persistent low-level stratus decks [*Horel and Cornejo-Garrido*, 1986; *Bendix and Lauer*, 1992].

[13] Heavy precipitation and severe floods also affect the coastal area of Ecuador during El Niño events, with rainfall differences between normal years and El Niño events as large as 200% for Guayaquil (Guayas Basin). Extensive precipitation during El Niño years occurs during the normal rainy season when the Hadley circulation is increased, and the ITCZ is displaced southward because of the strong warming of the Niño 1 + 2 region (0°S–10°S, 90°W–80°W (Figure 1d)) [*Rossel et al.*, 1996; *Bendix and Bendix*, 2006].

3. Methods

3.1. Stratigraphic Framework (ODP Site 1239 and Site MD02-2529)

[14] Sampling of Site 1239 followed the meters composite depth scale that was developed for the multiple offset cores [*Shipboard Scientific Party*, 2003]. The age model of the uppermost ~17.4 m, representing the past ~500 kyr, is based on oxygen isotope stratigraphy. We correlated the δ^{18}O record of the benthic foraminifera *Cibicidoides wuellerstorfi* to the chronology of the LR04 stack [*Lisiecki and Raymo*, 2005] using the AnalySeries software [*Paillard et al.*, 1996] (Figure 2). Sedimentation rates range from ~2 to ~5 cm kyr^{-1}, with higher values occurring during interglacials (Figure 2). Stratigraphy at Site MD02-2529 over the past three climatic cycles is based on the benthic δ^{18}O record performed on *C. wuellerstorfi* and on a previously published chronostratigraphy for the last 90 kyr [*Leduc et al.*, 2007].

3.2. Paleoceanographic Proxies

3.2.1. Foraminifera Oxygen Isotopes

[15] We measured the stable oxygen isotope composition of the epibenthic foraminifer *Cibicidoides wuellerstorfi*, as well as of two planktonic foraminiferal species, the surface dweller *Globigerinoides ruber*, and the deep-dwelling *Globorotalia tumida*. Approximately 4 individuals of *C. wullerstorfi* and 10 individuals of each planktonic species were selected from the 315–355 μm and 355–400 μm fractions, respectively. Measurements of δ^{18}O were performed on a Finnigan 253 MS with a Kiel CARBO device at the Alfred-Wegener-Institut (AWI) (Bremerhaven, Germany) with an analytical reproducibility of ~0.08‰ for δ^{18}O. The oxygen isotope composition values were calibrated using the NBS-19 standard and are reported relative to the International Atomic Energy Agency Vienna Pee Dee Belemnite standard. The resolution of sampling was defined on the basis of a preliminary age model from biostratigraphy in order to obtain intervals of 1000 years or less for benthic foraminifera and of 3000 years for planktonic foraminifera. The δ^{18}O difference between *G. ruber* ss and *G. tumida* is used as a proxy for water column thermal stratification (D. Rincón-Martínez et al., Tracking the equatorial front in the eastern equatorial Pacific Ocean by the isotopic and faunal composition of planktonic foraminifera, submitted to *Marine Micropaleontology*, 2010).

3.2.2. Alkenones

[16] Alkenones are a series of long-chain (C_{37}, C_{38}, and C_{39}) unsaturated methyl and ethyl ketones synthesized mainly by *Emiliania huxleyi* and some other species of the class Prymnesiophyceae that live in the uppermost meters of the euphotic zone. To obtain the total lipid extract, freeze-dried sediments (~1 g) from ODP Site 1239 were solvent extracted with 25 mL dichloromethane at 75°C at a pressure of 80 bars on an accelerated solvent extractor (Dionex ASE 200) at the Christian Albrecht University of Kiel. An internal standard (cholestane [$C_{27}H_{48}$] and hexatriacontane [$C_{36}H_{74}$]) was added and used to quantify organic compounds. Aliquots (1%–5%) of the total lipid fractions were separated using a

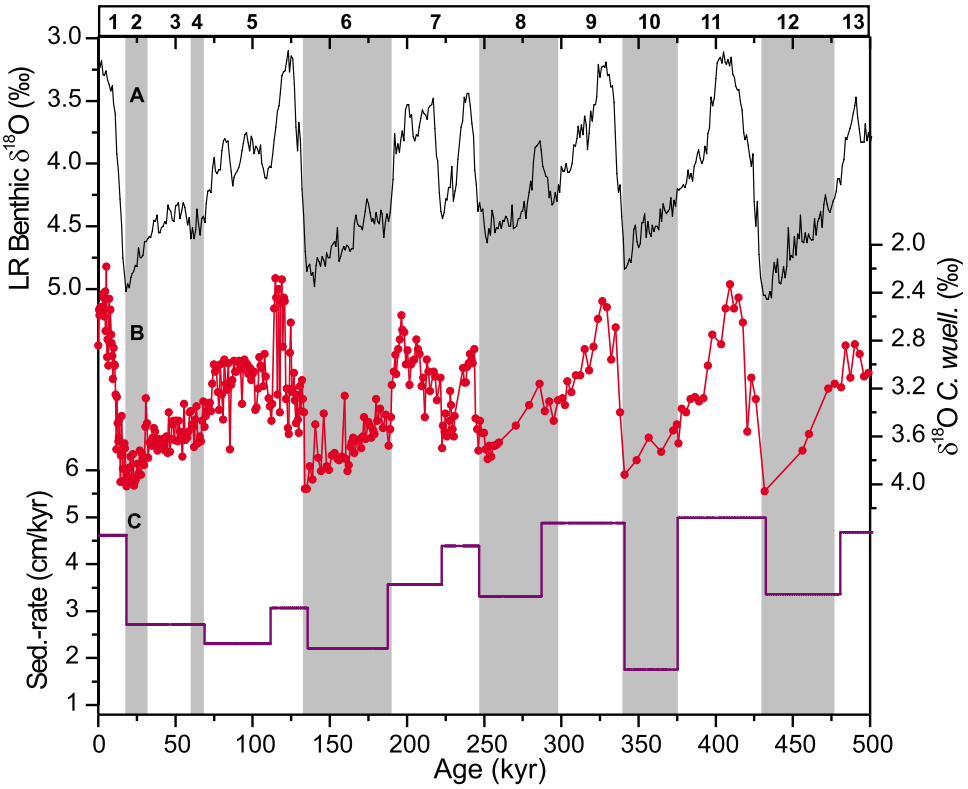

Figure 2. Oxygen isotope stratigraphy for the ODP Site 1239. (a) Benthic oxygen isotope stack [*Lisiecki and Raymo*, 2005]. (b) The δ^{18}O (‰) record of the benthic foraminifera *Cibicidoides wuellerstorfi* from ODP Site 1239. (c) Linear sedimentation rates (cm kyr^{-1}) of the uppermost ~17.4 m (past ~500 kyr) from ODP Site 1239. Shading highlights glacial marine isotopic stages.

double-column multidimensional gas chromatograph with two Agilent 6890 gas chromatographs for $C_{37:2}$ and $C_{37:3}$ alkenone identification and quantification. The procedure used at Centre Européen de Recherche et d'Enseignement des Géosciences de l'Environnement (Aix-Marseille Université) to extract and quantify $C_{37:2}$ and $C_{37:3}$ alkenones from MD02-2529 is fully described by *Sonzogni et al.* [1997] and *Pailler and Bard* [2002]. Alkenone-derived temperatures from MD02-2529 for the last 90 kyr have been previously published and discussed by *Leduc et al.* [2007]. The alkenone unsaturation index ($U^{K'}_{37}$) was calculated with the peak areas of the diunsaturated and triunsaturated C_{37} methyl alkenones using the ratio $(C_{37:2})/(C_{37:2} + C_{37:3})$. To reconstruct the SST, we used the alkenone unsaturation and the global calibration derived by *Müller et al.* [1998]:

$$U^{K'}_{37} = \langle 0.033 \times \mathrm{SST} \rangle + 0.044.$$

3.2.3. Foraminiferal Assemblage ($R_{c/d}$)

[17] The abundance ratio between *Globorotalia menardii cultrata* and *Neogloboquadrina dutertrei* (right coiling) has been used as an index for the influence of the Panama-Costa Rica Dome and the cold tongue upwelling systems and therefore is of value for locating the EF in the EEP [i.e., *Martinez and Bedoya*, 2001; *Martínez et al.*, 2006; Rincón-Martínez et al., submitted manuscript, 2010]. In this study we counted >300 specimens from the 355–400 μm size fraction, and the ratios were calculated according to Rincón-Martínez et al. (submitted manuscript, 2010):

$$R_{c/d} = \text{number of specimens of } \textit{G. cultrata} \,/(\text{number of specimens of } \textit{G. cultrata} + \textit{N. dutertrei})$$

3.3. Terrigenous Sediment Input

3.3.1. Siliciclastic Content

[18] The lithogenic record for ODP 1239 represents the residual sediment percentage obtained after subtraction of carbonate, opal, and organic matter:

$$\text{siliciclastic (wt \%)} = 100 - \%CaCO_3 - \%\text{biogenic opal} - \%\text{TOC}.$$

The determination of total organic carbon (TOC) was performed with the LECO technique (LECO Carbon-Sulfur Analyzer CS-125), and previous dissolution of the calcium carbonates was performed by adding 1 *M* solution of HCL to the dry sediment. Total carbon (TC) and total nitrogen (TN) were measured on the same TOC samples using a CNS elemental analyzer (Elementar Vario EL III). The carbonate content (wt %) was determined by the difference between TC and TOC:

$$CaCO_3(\text{wt \%}) = (\%\text{TC} - \%\text{TOC}) \times 8.33.$$

The concentration of biogenic silica (wt %) was quantified by using the automated leaching method according to *Müller and Schneider* [1993]. Biogenic opal was extracted from dry bulk sediment by using sodium hydroxide at ~85°C for ~45 min. The leaching solution was continuously analyzed for dissolved silicon by molybdenum-blue spectrophotometry. *DeMaster*'s [1981] mineral correction was consequently applied.

3.3.2. X-Ray Fluorescence Scanning and Inductively Coupled Plasma-Optical Emission Spectrometry Elemental Concentrations

[19] Elemental concentrations (unit is total elemental counts) were measured using an Avaatech^{TM} X-Ray Flourescence (XRF) Core Scanner (AWI, Bremerhaven) and a nondestructive measuring technique that allows rapid semiquantitative geochemical analysis of split sediment cores [*Richter et al.*, 2006]. Sampling intervals ranged from 1 to 5 cm, resulting in a time resolution of 200 and 400 years for the upper ~350 kyr of the XRF records and 1000 to 1500 years for the oldest part. Iron (Fe) and titanium (Ti) XRF counts were calibrated to absolute elemental concentration by using Inductively Coupled Plasma-Optical Emission Spectrometry. Previous to analysis, all samples were freeze-dried, and 34 discrete sediment samples were digested using HF (23 *M*), HNO_3 (15 *M*), and HCl (12 *M*). Measurements were carried out in a TJA-IRIS-Intrepid spectrometer at the geochemistry laboratories of AWI, and the results were used to convert XRF counts to element concentrations in mg g^{-1} of sediment by means of linear regressions ($r^2 = 0.83$, $n = 32$ for Fe and $r^2 = 0.63$, $n = 33$ for Ti).

3.3.3. Taraxerol

[20] Taraxerol has been reported to dominate the free and bound lipid composition inside *Rhizophora mangle* leaves and has been used to track past changes in mangrove ecosystems [*Versteegh et al.*, 2004; *Grosjean et al.*, 2007]. Total lipid extracts (see section 3.2.2) were methylated with diazomethane and silylated with N, O-bis (trimethylsilyl) trifluoroacetamide in pyridine and then analyzed by GC-MS (Trace GC-MS, Thermo Finnigan) at the Max-Planck-Institute for Marine Microbiology in Bremen. The relative abundance of taraxerol was estimated by peak integration in the mass chromatograms using a characteristic *m/z* value of 204 [*Killops and Frewin*, 1994; *Versteegh et al.*, 2004].

3.3.4. Mass Accumulation Rates

[21] Linear sedimentation rates (LSR; cm kyr^{-1}) and mass accumulation rates (AR) are derived from the calculated ages of individual samples along with the high-resolution-corrected bulk density (HROM; g cm^{-3}) based on borehole logging at Site 1239 [*Shipboard Scientific Party*, 2003]:

$$AR_{component} = \text{concentration component} \times \text{LSR} \times \text{HROM},$$

where AR is in ng cm^{-2} kyr^{-1} for the taraxerol, mg cm^{-2} kyr^{-1} for the iron and titanium, and g cm^{-2} kyr^{-1} for the bulk siliciclastic fraction.

4. Results and Discussion

4.1. Terrigenous Sediment Supply to the ODP Site 1239

[22] Terrigenous sedimentation supply at Site 1239 (Figure 3) is reconstructed from three independent proxy data sets: (1) AR of siliciclastic material, (2) high-resolution XRF core scanning (Fe, Ti), and (3) lipid biomarker taraxerol, indicative of the supply of plant debris from mangroves at the Ecuadorian coast.

[23] The terrigenous records at Site 1239 exhibit a consistent glacial-interglacial pattern over the past 500 kyr (Figures 3 and 4f). Sediments are predominantly terrigenous during interglacials, with siliciclastic contents generally above 50% and reaching maximum values of up to 80% during marine isotope stage (MIS) 7 (Figure 3b). Glacial siliciclastic contents are substantially lower, within the range of 20% to 40% with lowest values during MIS 2 and MIS 12. As siliciclastic contents may be substantially affected by productivity changes and carbonate dissolution, we calculated siliciclastic AR (Figure 3c) as a more reliable proxy for terrigenous supply changes. In line with higher sedimentation rates during interglacials (Figure 2c), the siliciclastic AR record reveals pronounced interglacial maxima with values 3 to 5 times higher than that found during glacials. Highest AR are found in MIS 7 and MIS 11, whereas MIS 5 values are relatively low, and minimum AR occur in MIS 10. Similar results are recorded in Fe and Ti AR records (Figures 3d–3g). The strong similarity between the Fe and Ti records suggests that diagenetic alteration potentially affecting Fe has not been a critical factor at Site 1239. Moreover, when log ratios of Fe and Ti over calcium (Ca) are computed to account for dilution by carbonates and nonlinearities between XRF counts and elemental concentrations [*Weltje and Tjallingii*, 2008], the first-order sign of changes in terrigenous supply on glacial-interglacial timescales remains unchanged (data not shown). Low AR of terrigenous components during MIS 5 indicate variable glacial-interglacial amplitudes in terrigenous supply to Site 1239. However, total siliciclastic, Fe, and Ti contents during MIS 5 are similar to other interglacials (Figures 3b, 3d, and 3f), and the low siliciclastic AR during MIS 5 are solely the result of low sedimentation rates.

[24] Glacial-interglacial siliciclastic AR variations at Site 1239 are unlikely due to postdepositional processes such as horizontal focusing or winnowing. According to *Lyle et al.* [2005], sediment focusing preferentially increases from elevated regions to the deeper parts of the basins, and in the Panama and Peru basins, the bulk sediment burial matches surface water patterns. Moreover, the observed glacial-interglacial pattern in local sediment supply to ODP Site 1239 demonstrates that continental rainfall rather than glacioeustatic sea level variations was the main factor controlling the basinward terrestrial transport off Ecuador. For example, during glacial times when the global sea level was at lowstand, one would expect an oceanward migration of fluvial depocenters and widespread fluvial incision of the subaerially exposed continental shelf producing increased siliciclastic AR at ODP Site 1239. In contrast, our records show higher concentrations and AR of terrigenous material during interglacials that overcompensated any potential sea level influence on fluvial sediment supply.

[25] High terrigenous AR during interglacial periods also contradict the concept that in the equatorial Pacific, transport of terrigenous material was increased during glacial periods [*Anderson et al.*, 2006; *McGee et al.*, 2007; *Winckler*

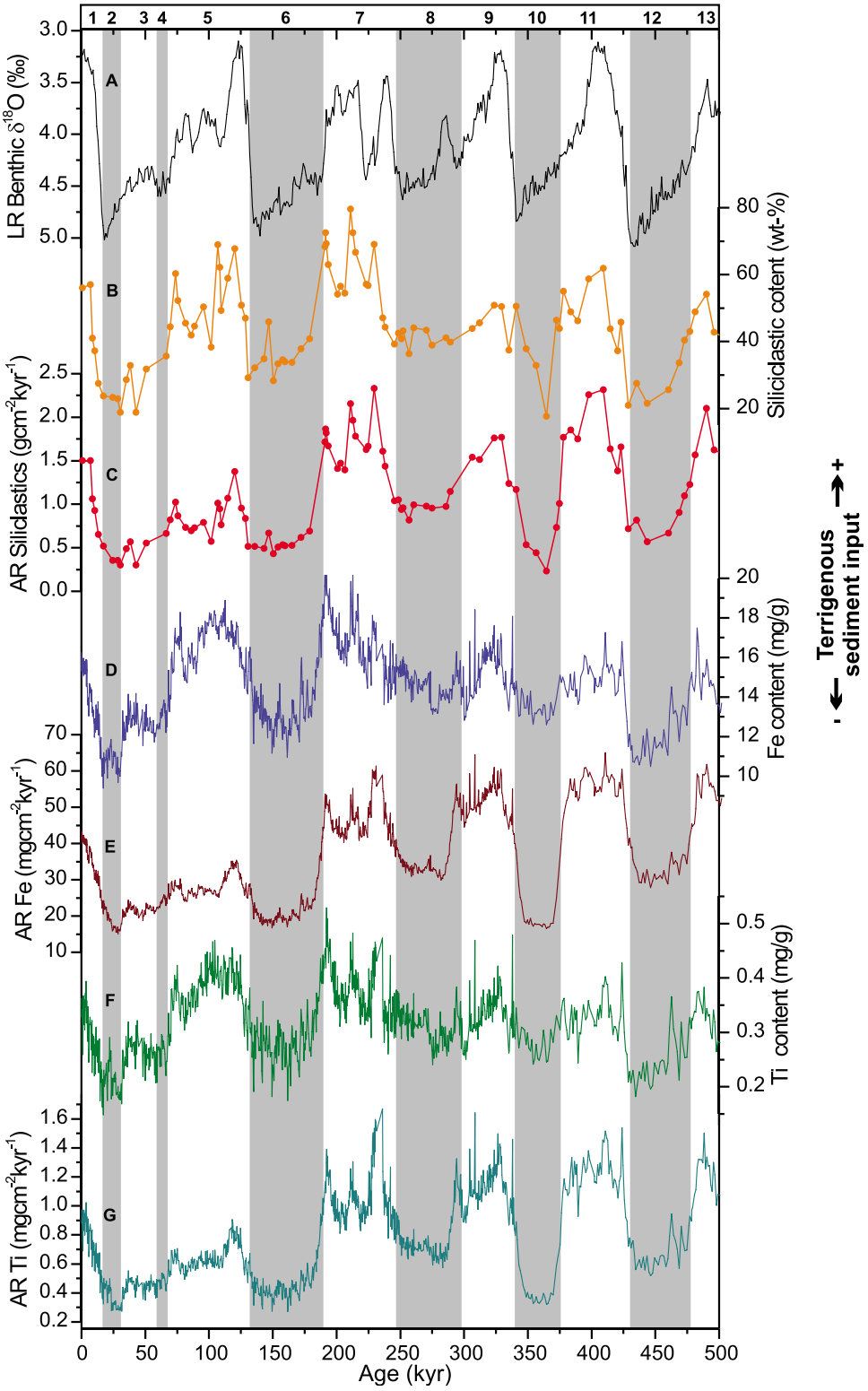

Figure 3. Records of changes in terrigenous sediment input to ODP Site 1239 over the last 500 kyr. (a) Benthic oxygen isotope stack [*Lisiecki and Raymo*, 2005] for stratigraphic reference. (b) Content (wt %) and (c) accumulation rates (AR, g cm^{-2} kyr^{-1}) of siliciclastics. (d) Iron contents (mg g^{-1}). (e) Iron AR (mg cm^{-2} kyr^{-1}). (f) Titanium contents (mg g^{-1}). (g) Titanium AR (mg cm^{-2} kyr^{-1}).

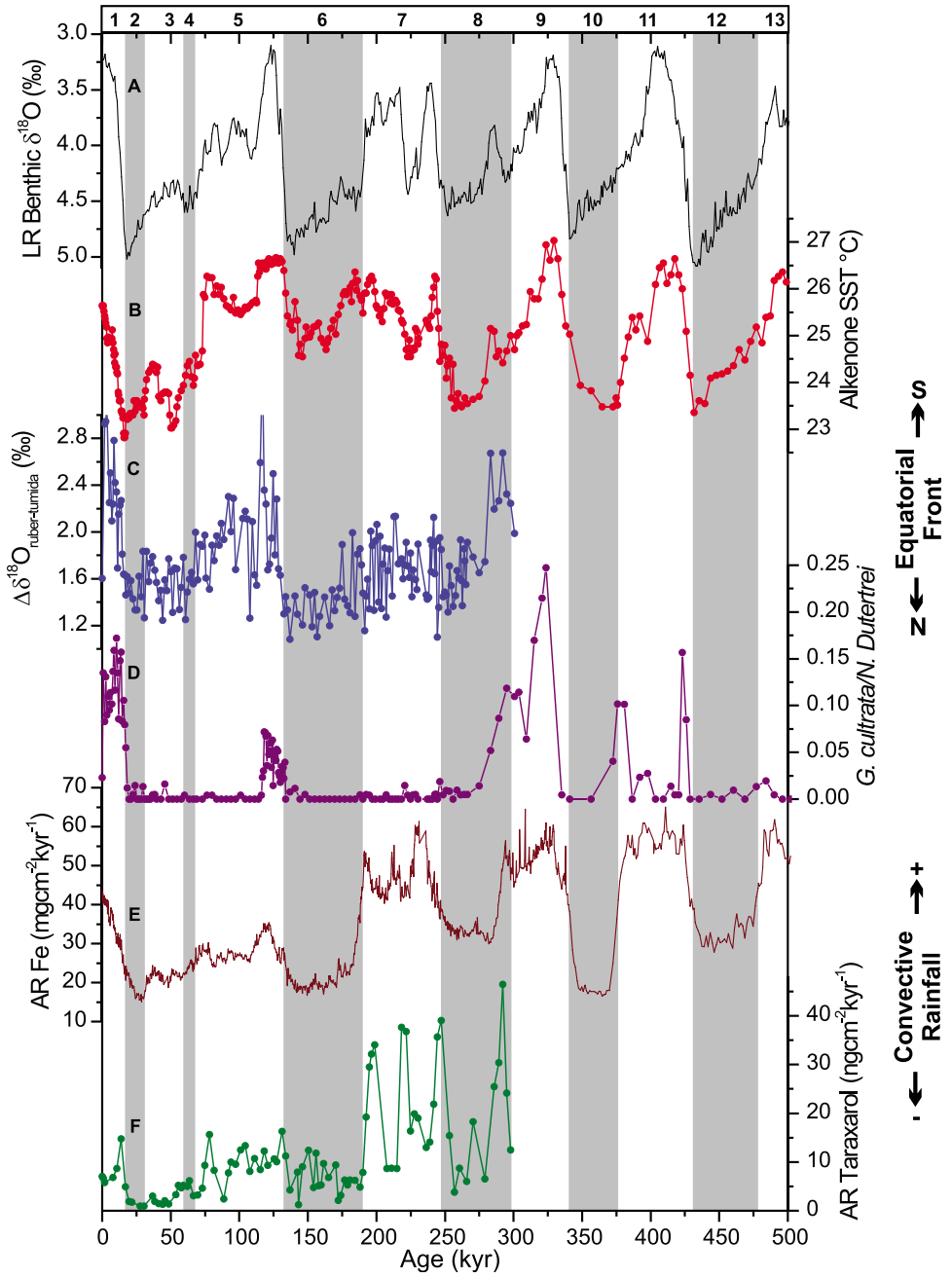

Figure 4. EEP paleoceanographic changes as reconstructed at ODP Site 1239. (a) Benthic oxygen isotope stack [*Lisiecki and Raymo*, 2005] for stratigraphic reference. (b) Alkenone sea surface temperature (SST) record. (c) $\Delta\delta^{18}O$ between *Globorotalia tumida* and *Globigerinoides ruber*. High values are indicative of strongly stratified waters north of the equatorial front. (d) Abundance ratio ($R_{c/d}$) between planktonic foraminifera *Globorotalia cultrata* and *Neogloboquadrina dutertrei*. High values are indicative of warm waters north of the equatorial front. (e) Iron AR (mg cm^{-2} kyr^{-1}). (f) Taraxerol AR (ng cm^{-2} kyr^{-1}). High values are interpreted as enhanced fluvial runoff as a result of increased continental rainfall.

et al., 2008]. We attribute the contrasting results to the fact that far from shore, the terrigenous component of deep-sea sediments consists of eolian dust and that these fluxes were generally greater during glacial periods than during interglacials [*Mahowald et al.*, 1999; *Kohfeld and Harrison*, 2001]. Hence, the rather nearshore location of Site 1239 suggests that fluvial input from the Guayas and/or Esmeraldas drainage systems was increased during interglacial periods relative to glacial periods.

[26] Our third proxy for terrigenous input is taraxerol AR, which was used as a proxy for sedimentation of mangrove leaf remains (*Rhizophora*) that were washed offshore by

riverine runoff [*Versteegh et al.*, 2004; *Grosjean et al.*, 2007]. The *Rhizophora* genus is the dominant mangrove along the Colombian and Ecuadorian coasts. and its distribution is associated with the presence of warm waters and humid coastal conditions north of the EF [*Heusser and Shackleton*, 1994; *Neill*, 1999]. Compared to glacials, taraxerol AR are higher during the Holocene and MIS 5 and reach extremely high values during MIS 7 (Figure 4f). These higher interglacial AR are consistent with our interpretation of predominantly fluvial terrigenous input induced by enhanced tropical rainfall. However, the supply of mangrove material may also be affected by sea level changes. For instance, in the nearby Angola Bight, *Kim et al.* [2005] showed that high taraxerol contents during terminations I and II were controlled by global sea level rise resulting in strong shelf erosion supplying preexisting deposits of mangrove material. Additional support for deglacial sea level control on EEP mangrove input into marine sediments comes from pollen analyses [*Heusser and Shackleton*, 1994; *González et al.*, 2006] and Mn/Ca of planktonic foraminifera [*Klinkhammer et al.*, 2009], which display maxima in mangrove pollen and dissolved terrestrial input to coastal surface waters during the last deglaciation. Our record shows early maxima in taraxerol AR during terminations I, II, and particularly III (Figure 4f) while taraxerol levels remain high during the whole interglacial period. Hence, we suggest that increased taraxerol sedimentary fluxes during interglacials are driven to some extent by increased riverine runoff.

4.2. SST, EF Latitudinal Position, and Their Relationship to Continental Precipitation

[27] Global compilations of SST estimations from modern sediments indicate that alkenones unsaturation, $U^{K'}_{37}$, is almost linearly related to annual mean SST from 0 to 10 m water depth [*Müller et al.*, 1998; *Conte et al.*, 2006; *Prahl et al.*, 2006]. $U^{K'}_{37}$ sensitivity to temperature has been assessed in laboratory cultures [*Prahl and Wakeham*., 1987], and second-order mechanisms such as salinity and alkenones synthesized by thermocline-dwelling coccolithophorids or diagenetic alterations are known to play a minor role on the alkenone-SST signal (see review by *Conte et al.* [2006]). It is unclear, however, why alkenones that are produced during an often discrete and short period of the annual cycle are representative of annual mean SST [*Prahl et al.*, 2000].

[28] Alkenone-derived SST at Site 1239 reveals pronounced glacial-interglacial cycles, with temperatures ranging from ~22.8 during MIS 2 to ~27°C during MIS 9 (Figure 4b). We find SST amplitudes of up to 3.5°C for the oldest glacial-interglacial cycles (MIS 8–13), ~2.5°C for the MIS 8–7 transition, only ~2°C for termination II (MIS 6–5), and again higher amplitudes of ~3°C for termination I (MIS 2–1). The magnitude of the deglacial SST increase during termination I is consistent with previous studies conducted in the eastern tropical Pacific that used Mg/Ca ratios and faunal assemblages [*Lea et al.*, 2000; *Pena et al.*, 2008; *MARGO Project Members*, 2009]. Glacial-interglacial SST amplitudes in other $U^{K'}_{37}$ estimations from the region are, however, somewhat lower (~1°C to ~2°C) [*Horikawa et al.*, 2006; *Pahnke et al.*, 2007; *Koutavas and Sachs*, 2008; *Dubois et al.*, 2009]. Sea surface temperature values at Site MD02-2529 range from minima of ~25°C during MIS 2 and 8 to maxima of ~28°C during the Holocene (Figure 5b). Glacial-interglacial SST amplitudes are generally smaller than at Site 1239, on the order of 2°C for terminations I (MIS 2−1) and III (MIS 8−7) and less than 1°C for termination II (MIS 6−5).

[29] Comparison of the global benthic $\delta^{18}O$ record (LR04 stack) with the Site 1239 SST estimates reveals several interesting features: (1) an early warming is recorded prior to terminations I, III, and IV; (2) SSTs during MIS 6 are warmer than those recorded during the other glacial periods; (3) an abrupt cooling occurs during early MIS 3 and is followed by a warming of the same magnitude at the end of MIS 3; and (4) SST estimates recorded during the Holocene reveal ~1°C lower SST when compared to other interglacial periods (Figure 4b). The early warming during the glacial terminations is also observed in other tropical records (see review by *Schneider et al.* [1999]) and has been suggested to be linked with low-latitude insolation forcing. Elevated glacial SSTs during MIS 6 are also found at Site MD02-2529 (Figure 5b) in the eastern Pacific cold tongue [*Calvo et al.*, 2001] and in many other Indian and Atlantic equatorial records (see review by *Schneider et al.* [1999]). In contrast, EEP $\delta^{18}O$ and Mg/Ca records of planktonic foraminifera suggest a colder MIS 6 in comparison with alkenone-based SSTs with a cooling of similar magnitude to those found on the preceding and following glacial periods [e.g., *Lea et al.*, 2000; *Pena et al.*, 2008].

[30] Given the importance of tropical SST patterns in determining present-day Ecuadorian rainfall formation and associated fluvial discharges [i.e., *Rossel et al.*, 1996; *Bendix and Bendix*, 2006] (Figures 1b–1d), past SST changes offshore Ecuador likely impacted the terrigenous material fluxes at ODP Site 1239. On the basis of this modern SST-rainfall correlation (Figure 1d), the range of glacial-interglacial SSTs plausibly resulted in substantial precipitation changes in coastal Ecuador (e.g., more than doubling of rainfall for the glacial-interglacial increase from 23.5°C to 26.5°C). Thus, we infer that higher accumulation of lithogenic sediments at Site 1239 generally reflects higher fluvial input and a wetter Ecuadorian coast, most likely coupled to warmer SSTs in combination with southward shifts of the EF-ITCZ system as observed today during austral summer or during El Niño years. Lower lithogenic accumulations during glacial periods indicate decreased fluvial input and arid conditions on the continent.

[31] Further support for EF-ITCZ southward excursions during interglacials comes from the $\delta^{18}O$ gradient between planktonic foraminifera living at different depths (hereafter referred to as $\Delta\delta^{18}O$) (Figure 4c) and the $R_{c/d}$ index (Figure 4d). Planktonic foraminifera $\Delta\delta^{18}O$ is indicative of water column stratification in the EEP (Rincón-Martínez et al., submitted manuscript, 2010). High interglacial $\Delta\delta^{18}O_{G.\ ruber-G.\ tumida}$ values (Figure 4c) indicate stratified waters north of the EF, where a strong thermal gradient occurs in the upper 100 m. Low glacial $\Delta\delta^{18}O_{G.\ ruber-G.\ tumida}$ values reflect intensified upwelling linked to a stronger Peru Current and a northward location of the EF-ITCZ complex. With the exception of MIS 7, glacial-interglacial patterns are also evident in the $R_{c/d}$ record (Figure 4d),

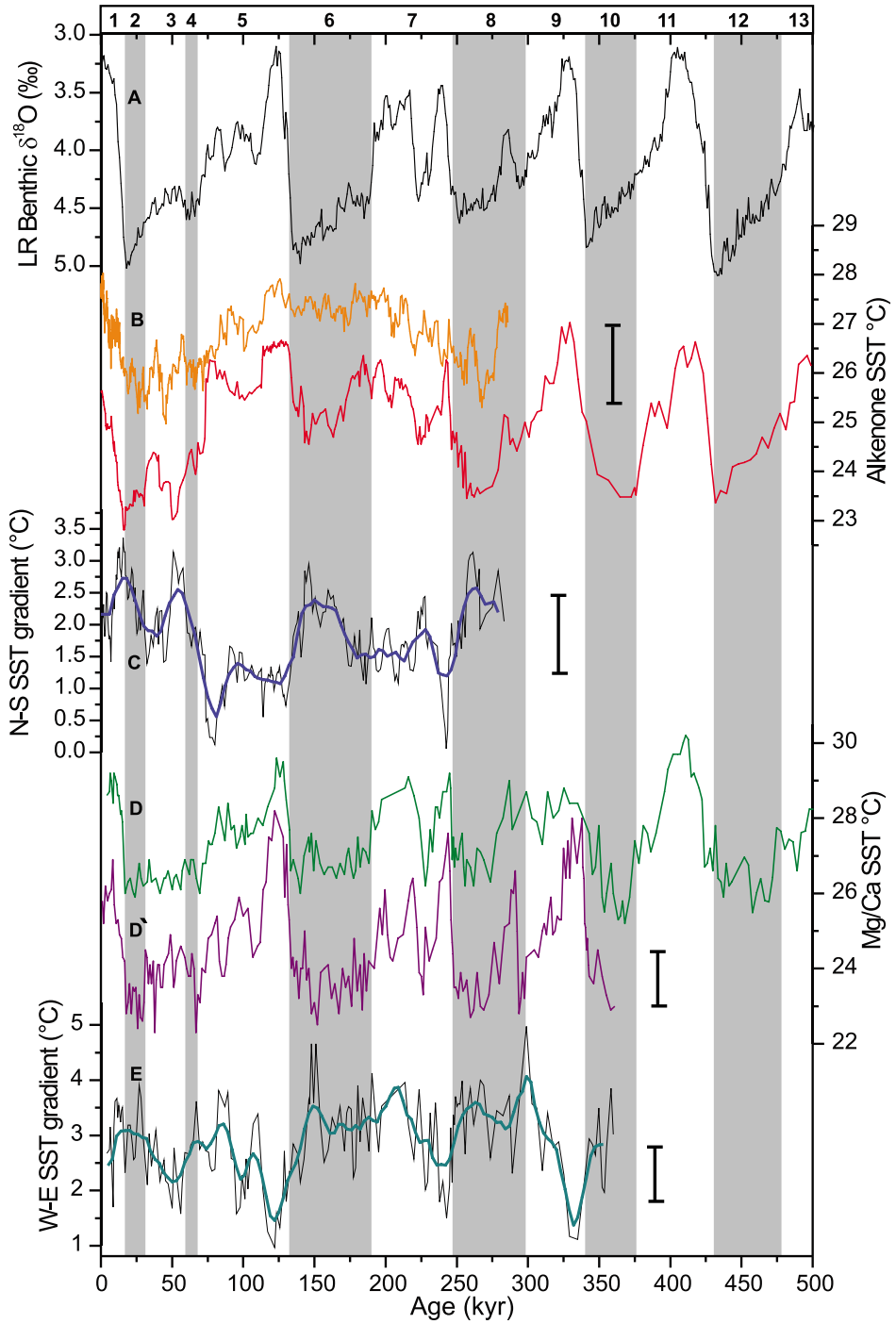

Figure 5. Comparison of eastern and western equatorial Pacific SST records. (a) Benthic oxygen isotope stack [*Lisiecki and Raymo*, 2005] for stratigraphic reference. (b) Alkenone-derived SST records from the two eastern equatorial Pacific sites. MD02-2529 (top line, this study) data represent the eastern Pacific warm pool; ODP Site 1239 data (bottom line, this study) represent the northernmost reach of the cold tongue. (c) SST gradient between the northern Site MD02-2529 (08°12.33′N) and the southern Site 1239 (0°40.32′S). Increased SST difference between the equator and the eastern Pacific warm pool represents La Niña-like mean conditions. (d) Mg/Ca SST record from ODP Site 806B (0°19.1′N, 159°21.7′E; top line) in the western Pacific warm pool [*Medina-Elizalde and Lea*, 2005] and Site TR163-19 (2°15′S, 90°57′W; bottom line) from north of the EEP cold tongue [*Lea et al.*, 2000]. (e) SST gradient between the eastern and western tropical Pacific sites. Reduced west-east SST gradients represent El Niño-like mean conditions.

which exhibits higher values during interglacials, indicating southward shifts of the EF-ITCZ. Low and minimum $R_{c/d}$ values recorded during MIS 5 and 7, respectively, are attributed to potential changes on ecologic factors such as food web or nutrient supply that might also exert control on the abundance of *G. cultrata* [i.e., *Martinez and Bedoya*, 2001; *Martínez et al.*, 2006; Rincón-Martínez et al., submitted manuscript, 2010].

[32] Glacial-interglacial relation of enhanced fluvial input patterns and thus tropical precipitation of coastal Ecuador to warmer offshore SSTs appears to be a robust feature. But low siliciclastic AR during MIS 5 (Figures 4b and 4e) and low $\Delta\delta^{18}O_{G.\ ruber-G.\ tumida}$ and $R_{c/d}$ values during MIS 7 beg the question of whether there is a consistent signature of rainfall response to the SST forcing. The specific mechanism behind the disproportion in the magnitude of lithogenic supply among interglacials is unknown. Differences in atmospheric CO_2 concentrations, astronomical forcing, and glacial ice volume [see *Tzedakis et al.*, 2009] plausibly fostered variations in moisture advection to the ITCZ and to the continent, stimulating variations in precipitation, vegetation cover, and fluvial suspended loads that are reflected in the variable magnitude between the different interglacials of terrestrial input to the EEP.

4.3. Changes of Equatorial Pacific Mean States During the Last 300,000 Years

[33] Tropical Pacific SST patterns translate into transequatorial and cross-equatorial equatorial pressure gradients that control the position and intensities of atmospheric convection over the Pacific Ocean. We apply this concept and investigate past changes in zonal and meridional SST gradients (Figures 5c and 5e) as indication of changes in the large-scale tropical atmospheric circulation, notably, the Walker and Hadley cells. The zonal SST gradient was estimated using published *Globigerinoides ruber* Mg/Ca measured at ODP Site 806B from the Ontong Java Plateau (0°19.1′N, 159°21.7′E, 2520 m water depth) [*Medina-Elizalde and Lea*, 2005] and at Site TR163-19 (2°15′S, 90°57′W, 2348 m water depth) just north of the EEP cold tongue [*Lea et al.*, 2000]. The meridional gradient was calculated using alkenone-derived SST from ODP Site 1239 and Site MD02-2529 (this study). Here we use the terms "El Niño-like" and "La Niña-like" to describe mean changes in the zonal and meridional SST gradients across the equatorial Pacific, either in the form of decreased (El Niño) or increased (La Niña) gradients without specifically implying changes in frequency or amplitude of ENSO variability.

[34] Previous studies comparing SST derived from alkenones and Mg/Ca in the EEP have reported contrasting results. For example, on millennial-scale alkenones and Mg/Ca SST, changes that have punctuated the last deglaciation are known to be out of phase [i.e., *Mix*, 2006; *Koutavas and Sachs*, 2008]. Other studies based on compilations of Holocene SST data have revealed divergent SST trends over the last 10 kyr, with warming versus cooling recorded by alkenone- versus Mg/Ca-based SST, respectively [i.e., *Leduc et al.*, 2010; *Sachs*, 2008; *Sachs et al.*, 2000]. These dissimilarities suggest that coccolithophorids and foraminifera do not record the same paleoceanographic features. For this reason we avoided using different proxies when we compiled the zonal and meridional SST gradients across the equatorial Pacific, and we assumed that these gradients best represent past changes in the equatorial SST mean state. Reported error bars in alkenone and Mg/Ca temperature estimates are ±1.5°C and ±0.6°C, respectively [*Müller et al.*, 1998; *Lea et al.*, 2000].

[35] The zonal SST gradient shows a distinct glacial-interglacial pattern, with minima during the interglacials and maxima during glacials (Figure 5e). For instance, during MIS 5e, MIS 7e, and MIS 9e the west-east SST gradient was ~1.5°C, while for MIS 2 and MIS 8 it was ~3°C and ~3.5°C, respectively. This suggests a weakened Walker circulation (El Niño-like conditions) during interglacials and intensified Walker circulation (La Niña-like conditions) during glacial periods. Such a scenario is consistent with reduced upwelling activity or intensity, an anomalous warming in the easternmost Pacific, an EF-ITCZ southward migration, and heavy rainfall on the Guayas and Esmeraldas basins during interglacials (Figure 3) [i.e., *Horel and Cornejo-Garrido*, 1986; *Hastenrath*, 2002; *Rossel et al.*, 1996; *Bendix and Bendix*, 2006].

[36] Systematic glacial-interglacial patterns are also recorded in the meridional SST gradient record (Figures 5b and 5c). Low meridional SST gradients occur during MIS 5 (0.8°C to1.4°C) and MIS 7 (1.4°C to 1.8°C) while MIS 2, 4, 6, and 8 were characterized by a steeper SST gradient (2.2°C to 2.6°C). Today, the annual mean position of the eastern Pacific ITCZ is located in the vicinity of 10°N and remains north of the equator because of a strong cross-equatorial SST gradient. During El Niño years, mainly during the months of March and April, the meridional gradient is weakened, leading to extensive precipitation over coastal Ecuador linked to an equatorward shift of the meridional position of the ITCZ. Taken together, the co-occurrence of weaker meridional and zonal SST gradients suggests an El Niño-like state during interglacial periods contrasting with La Niña-like conditions recorded during glacial periods. This result is consistent with reconstructions of the ENSO, suggesting reduced ENSO activity during the Last Glacial Maximum (LGM) [*Leduc et al.*, 2009]. Sea surface temperature reconstructions from the southeastern Pacific margin suggest that remote advection of cold waters from high latitudes is a valid mechanism for explaining the observed glacial La Niña-like state [*Kaiser et al.*, 2005].

[37] The zonal SST gradient is particularly well expressed during peak interglacials (i.e., MIS 5e, MIS 7e, and MIS 9e), while it does not show much change between late interglacials and glacials. In contrast, the meridional SST gradient clearly mimics glacial-interglacial patterns. One explanation for the disparate pattern of zonal and meridional SST gradients is that the zonal SST gradient was estimated from *G. ruber* Mg/Ca measurements, while the meridional SST gradient was calculated from alkenone ratios. The signal offset between both SST gradients might reflect contrasting sensitivities to different seasonal/interannual variations or depth distribution of proxy carriers [i.e., *Mix*, 2006; *Leduc et al.*, 2010], rather than disentanglement of the Hadley and Walker circulations. Alternatively, possible long-term

modifications of the tropical Pacific mean state, such as migration of the main centers of deep convection, could explain the divergent patterns of SST gradients, plausibly in conjunction with nonconventional El Niño, namely, the El Niño-modoki or pseudo-El Niño [i.e., *Yeh et al.*, 2009]. During such anomalous conditions, the maximum SST anomaly persists in the central Pacific, sandwiched between anomalous cooling in the east and west, modifying the atmospheric circulation and resulting in distinctly different global impacts than conventional El Niño conditions.

4.4. Comparison to Previous Paleoceanographic and Paleoclimatic Studies From the EEP and Adjacent South American Continent

[38] Our findings contradict the common view that during glacial times, the location of tropical rainfall zones experienced a southward displacement globally. Modeling studies simulate a southward displacement of the marine ITCZ in response to changes in continental ice volume at high latitudes [*Yin and Battisti*, 2001; *Chiang et al.*, 2003; *Chiang and Bitz*, 2005; *Broccoli et al.*, 2006]. However, today's climatology and variability of the eastern tropical Pacific SST have proven difficult to reproduce, even with current state-of-the-art coupled ocean-atmosphere general circulation models [*Mechoso et al.*, 1995; *Wang et al.*, 2005; *Wittenberg et al.*, 2006]. For instance, in simulations of the seasonal cycle, the modeled ITCZ tends to move across the equator following the seasonal movement of the Sun rather than remaining in the Northern Hemisphere as is suggested by monthly monitoring (i.e., http://trmm.gsfc.nasa.gov/). Moreover, in the current models, the ITCZ persists too long at a southern position compared to observations, causing a double ITCZ in the annual mean. Therefore, numerical models appear to overestimate the control of Northern Hemisphere ice sheets on the ITCZ and do not adequately implement low latitude air-sea interactions.

[39] Our results also challenge previous suggestions that a glacial relaxation of the SST asymmetry across the equator and a southward displacement of the marine ITCZ in the eastern Pacific were likely reflecting an El Niño-like pattern [*Koutavas et al.*, 2002; *Koutavas and Lynch-Stieglitz*, 2003]. Alternatively, the LGM reduction in the meridional $\delta^{18}O$ gradient reconstructed by *Koutavas and Lynch-Stieglitz* [2003] can be interpreted in terms of a northward migration of the EF-ITCZ system because their records are located primarily on the seasonal path of the EF-ITCZ system. Thus, a glacial northward shift of the EF would cause weaker meridional $\delta^{18}O$ gradients because of minimum changes in SST and salinity within the cold tongue. Other eastern Pacific alkenone-SST reconstructions [i.e., *Calvo et al.*, 2001; *Liu and Herbert*, 2004; *Horikawa et al.*, 2006; *Pahnke et al.*, 2007; *Koutavas and Sachs*, 2008; *Dubois et al.*, 2009], together with previous SST estimates based on marine microfossils [i.e., *Pisias and Mix*, 1997; *Feldberg and Mix*, 2003; *Martínez et al.*, 2003], support this view by demonstrating that sites located south of the EF experienced stronger cooling during the LGM and stronger warming during the last deglaciation compared to sites located north of the EF.

[40] Paleoclimate records from South America indicate southward ITCZ displacements during Northern Hemisphere ice sheet expansions (i.e., Amazon Basin [*Wang et al.*, 2004; *Jacob et al.*, 2007], Bolivian Altiplano [*Baker et al.*, 2001], Venezuela [*Rull*, 1996], ice cores [*Thompson et al.*, 1998; *Bradley et al.*, 2003], and glaciers [*Heine*, 2000]). This is in opposition to what is indicated by our marine data. The divergent behavior of the ITCZ in the continent plausibly relates to differences in heat flux patterns over the relatively dry continent as compared to the ocean where meridional temperature gradients were more prominent. This results in latitudinal ITCZ migrations over the continent that are much larger over the Amazon Basin and the Altiplano, while at the same time the ITCZ position over the EEP is defined by the geometry of the cold tongue-EF complex and the subtropical gyre circulation [i.e., *Horel et al.*, 1989; *Poveda et al.*, 2006; *Garreaud et al.*, 2009].

5. Summary and Conclusions

[41] We find prominent glacial-interglacial changes of fluvial sediment input that reflects more humid conditions along the Ecuadorian coast during interglacials. A warmer interglacial EEP cold tongue and a southward shift of the EF-ITCZ system likely control these humid interglacial conditions. Conversely, reduced fluvial input during glacials suggests more arid conditions coinciding with larger tropical Pacific SST gradients and a more northward location of the EF-ITCZ system. Despite this general tight coupling of rainfall changes in Ecuador to offshore oceanographic conditions, there are distinct differences between the individual interglacials, plausibly reflecting offsets in precipitation as well as duration and variability of interglacial climates of the past 500,000 years. Numerical modeling is required to test the sensitivity of past interglacial conditions and, notably, the distribution and intensity of tropical rainfall to variable atmospheric CO_2 concentrations, glacial ice volume, and orbital forcing.

[42] Zonal SST gradients in the eastern Pacific are reduced throughout interglacials and enhanced during glacials. With regards to long-term changes in the mean climate state, our data suggest a predominance of El Niño-like conditions off Ecuador during interglacials, while glacial conditions seem to more closely mimic La Niña-like conditions.

[43] Contrary to climate models our data indicate a northern EF-ITCZ position during glacials in the EEP. This was plausibly favored by the facts that (1) the cross-equatorial SST asymmetry was enhanced with stronger cooling south of the EF, which would drive the southeasterly trade winds across the equator, displacing the ITCZ to a northerly position [i.e., *Calvo et al.*, 2001; *Liu and Herbert*, 2004; *Horikawa et al.*, 2006; *Dekens et al.*, 2007; *Pahnke et al.*, 2007; *Koutavas and Sachs*, 2008; *Dubois et al.*, 2009; this study]; (2) the southeast-to-northwest tilted coastal geometry has not changed during the last 500 kyr, promoting coastal upwelling predominantly active south of the equator; and (3) the influence of the Andes and the South Pacific subtropical anticyclone on the regional atmospheric circulation remained reasonably stable during the entire time span, keeping the ocean surface cool through evaporation and suppressing deep convection in the Southern Hemisphere [e.g., *Takahashi and Battisti*, 2007].

[44] The glacial-interglacial latitudinal shifts of the EF-ITCZ system suggested by our data may be restricted to the EEP and the coastal area of northwest South America. Glacial cooling is particularly pronounced in the southeast Pacific [e.g., *Kaiser et al.*, 2005], which suggests a possibility that ITCZ migration in the region may be controlled by the northward advection of cold waters with the Humboldt Current system. Conversely, in the central and western Pacific, the magnitude of the cross-equatorial pressure gradient diminishes because the broad western Pacific warm pool dominates the SST pattern, leading to a potentially wider latitudinal range for ITCZ migrations during glacial times. Over the South American continent, away from the coast, the Andes and Amazon Basin impact atmospheric circulation patterns, allowing larger southward migrations of the ITCZ during glacial periods.

[45] **Acknowledgments.** At AWI, Reza Ahi assisted with TOC, opal, and CNS analyses and Lisa Schönborn provided invaluable assistance with oxygen isotopic measurement. Funding was provided through the German Science Foundation (grants Ha 2756/9-1 and TI240/17-2). D.R.M. and S.C. acknowledge Marcel Kuypers for his interest and support of this project and Gail Lee Arnold for her editorial comments. The authors further thank Frauke Rostek (CEREGE), who generated a considerable amount of alkenones data for Site MD02-2529, and Silvia Koch for her assistance at the biomarker laboratory at the CAU-IfG. This research used samples provided by the Integrated Ocean Drilling Program/Ocean Drilling Program (IODP/ODP) and the IMAGES program. Editorial comments by Rainer Zahn and critical reviews by George Philander and two anonymous reviewers substantially improved this manuscript.

References

Amador, J. A., E. J. Alfaro, O. G. Lizano, and V. O. Magaña (2006), Atmospheric forcing of the eastern tropical Pacific, *Prog. Oceanogr.*, *69*, 101–142, doi:10.1016/j.pocean.2006.03.007.

Anderson, R. F., M. Q. Fleisher, and Y. Lao (2006), Glacial-interglacial variability in the delivery of dust to the central equatorial Pacific Ocean, *Earth Planet. Sci. Lett.*, *242*, 406–414, doi:10.1016/j.epsl.2005.11.061.

Andreasen, D. J., and A. C. Ravelo (1997), Tropical Pacific Ocean thermocline depth reconstructions for the Last Glacial Maximum, *Paleoceanography*, *12*, 395–413, doi:10.1029/97PA00822.

Andreasen, D. J., A. C. Ravelo, and A. J. Broccoli (2001), Remote forcing at the Last Glacial Maximum in the tropical Pacific Ocean, *J. Geophys. Res.*, *106*, 879–897, doi:10.1029/1999JC000087.

Baker, P. A., G. O. Seltzer, S. C. Fritz, R. B. Dunbar, M. J. Grove, P. M. Tapia, S. L. Cross, H. D. Rowe, and J. P. Broda (2001), The history of South American tropical precipitation for the past 25,000 years, *Science*, *291*, 640–643, doi:10.1126/science.291.5504.640.

Bendix, J. (2000), Precipitation dynamics in Ecuador and northern Peru during the 1991/92 El Niño: A remote sensing perspective, *Int. J. Remote Sens.*, *21*, 533–548, doi:10.1080/014311600210731.

Bendix, A., and J. Bendix (2006), Heavy rainfall episodes in Ecuador during El Niño events and associated regional atmospheric circulation and SST patterns, *Adv. Geosci.*, *6*, 43–49.

Bendix, J., and W. Lauer (1992), Die Niederschlagsjahreszeiten in Ecuador und ihre Klimatdynamische interpretation, *Erdkunde*, *46*, 118–134, doi:10.3112/erdkunde.1992.02.04.

Bradley, R. S., M. Vuille, D. Hardy, and L. G. Thompson (2003), Low latitude ice cores record Pacific sea surface temperatures, *Geophys. Res. Lett.*, *30*(4), 1174, doi:10.1029/2002GL016546.

Broccoli, A. J., K. A. Dahl, and R. J. Stouffer (2006), Response of the ITCZ to Northern Hemisphere cooling, *Geophys. Res. Lett.*, *33*, L01702, doi:10.1029/2005GL024546.

Calvo, E., C. Pelejero, J. C. Herguera, A. Palanques, and J. O. Grimalt (2001), Insolation dependence of the southeastern subtropical Pacific sea surface temperature over the last 400 kyr, *Geophys. Res. Lett.*, *28*, 2481–2484, doi:10.1029/2000GL012024.

Cane, M. A. (2004), The evolution of El Niño, past and future, *Earth Planet. Sci. Lett.*, *230*, 227–240, doi:10.1016/j.epsl.2004.12.003.

Chiang, J. C. H., and C. M. Bitz (2005), Influence of high latitude ice cover on the marine Intertropical Convergence Zone, *Clim. Dyn.*, *25*, 477–496, doi:10.1007/s00382-005-0040-5.

Chiang, J. C. H., M. Biasutti, and D. S. Battisti (2003), Sensitivity of the Atlantic Intertropical Convergence Zone to Last Glacial Maximum boundary conditions, *Paleoceanography*, *18*(4), 1094, doi:10.1029/2003PA000916.

Clement, A. C., R. Seager, and M. A. Cane (1999), Orbital controls on the El Niño-Southern Oscillation and the tropical climate, *Paleoceanography*, *14*, 441–456, doi:10.1029/1999PA900013.

Conkright, M. E., R. A. Locarnini, H. E. Garcia, T. D. O'Brien, T. P. Boyer, C. Stephens, and J. I. Antonov (2002), World Ocean Atlas 2001: Objective analyses, data statistics, and figures, CD-ROM documentation, *Internal Rep. 17*, Natl. Oceanogr. Data Cent., NOAA, Silver Spring, Md.

Conte, M. H., M.-A. Sicre, C. Rühlemann, J. C. Weber, S. Schulte, D. Schulz-Bull, and T. Blanz (2006), Global temperature calibration of the alkenone unsaturation index (U) in surface waters and comparison with surface sediments, *Geochem. Geophys. Geosyst.*, *7*, Q02005, doi:10.1029/2005GC001054.

Dekens, P. S., A. C. Ravelo, and M. D. McCarthy (2007), Warm upwelling regions in the Pliocene warm period, *Paleoceanography*, *22*, PA3211, doi:10.1029/2006PA001394.

DeMaster, D. J. (1981), Measuring biogenic silica in marine sediments and suspended matter, in *Marine Particles: Analysis and Characterization*, *Geophys. Monogr. Ser.*, vol. 63, edited by D. C. Hurd and D. W. Spenser, pp. 363–368, AGU, Washington, D. C.

de Szoeke, S. P., S.-P. Xie, T. Piyama, K. J. Richards, and R. J. O. Small (2007), What maintains the SST front north of the eastern Pacific equatorial cold tongue?, *J. Clim.*, *20*, 2500–2514, doi:10.1175/JCLI4173.1.

Dubois, N., M. Kienast, C. Normandeau, and T. D. Herbert (2009), Eastern equatorial Pacific cold tongue during the Last Glacial Maximum as seen from alkenone paleothermometry, *Paleoceanography*, *24*, PA4207, doi:10.1029/2009PA001781.

Fedorov, A. V., P. S. Dekens, M. McCarthy, A. C. Ravelo, P. B. deMenocal, M. Barreiro, R. C. Pacanowski, and S. G. Philander (2006), The Pliocene Paradox (mechanisms for a permanent El Niño), *Science*, *312*, 1485–1489, doi:10.1126/science.1122666.

Feldberg, M. J., and A. C. Mix (2003), Planktonic foraminifera, sea surface temperatures, and mechanisms of oceanic change in the Peru and south equatorial currents, 0–150 ka BP, *Paleoceanography*, *18*(1), 1016, doi:10.1029/2001PA000740.

Fiedler, P. C., and L. D. Talley (2006), Hydrography of the eastern tropical Pacific: A review, *Prog. Oceanogr.*, *69*, 143–180, doi:10.1016/j.pocean.2006.03.008.

Fiedler, P. C., V. Philbrick, and F. P. Chavez (1991), Oceanic upwelling and productivity in the eastern tropical Pacific, *Limnol. Oceanogr.*, *36*(8), 1834–1850, doi:10.4319/lo.1991.36.8.1834.

Garreaud, R. D., M. Vuille, R. Compagnucci, and J. Marengo (2009), Present-day South American climate, *Palaeogeogr. Palaeoclimatol. Palaeoecol.*, *281*, 180–195, doi:10.1016/j.palaeo.2007.10.032.

González, C., L. E. Urrego, and J. I. Martínez (2006), Late Quaternary vegetation and climate change in the Panama Basin: Palynological evidence from marine cores ODP 677B and TR 163–38, *Palaeogeogr. Palaeoclimatol. Palaeoecol.*, *234*, 62–80, doi:10.1016/j.palaeo.2005.10.019.

Grosjean, E., G. A. Logan, N. Rollet, G. J. Ryan, and K. Glenn (2007), Geochemistry of shallow tropical marine sediments from the Arafura Sea, Australia, *Org. Geochem.*, *38*, 1953–1971, doi:10.1016/j.orggeochem.2007.06.017.

Hastenrath, S. (2002), The Intertropical Convergence Zone of the eastern Pacific revisited, *Int. J. Climatol.*, *22*, 347–356, doi:10.1002/joc.739.

Heine, K. (2000), Tropical South America during the Last Glacial Maximum: Evidence from glacial, periglacial and fluvial records, *Quat. Int.*, *72*, 7–21, doi:10.1016/S1040-6182(00)00017-3.

Heusser, L. E., and N. J. Shackleton (1994), Tropical climatic variation on the Pacific slopes of the Ecuadorian Andes based on a 25,000 year pollen record from deep-sea sediment core Tri163-31B, *Quat. Res.*, *42*, 222–225, doi:10.1006/qres.1994.1072.

Horel, J. D., and A. G. Cornejo-Garrido (1986), Convection along the coast of northern Peru during 1983: Spatial and temporal variations of clouds and rainfall, *Mon. Weather Rev.*, *114*, 2091–2105, doi:10.1175/1520-0493(1986)114<2091:CATCON>2.0.CO;2.

Horel, J. D., A. N. Hahmann, and J. E. Geisler (1989), An investigation of the annual cycle of convective activity over the tropical Americas, *J. Clim.*, *2*, 1388–1403, doi:10.1175/1520-0442(1989)002<1388:AIOTAC>2.0.CO;2.

Horikawa, K., M. Minagawa, M. Murayama, Y. Kato, and H. Asahi (2006), Spatial and temporal sea-surface temperatures in the eastern equatorial Pacific over the past 150 kyr, *Geophys. Res. Lett.*, *33*, L13605, doi:10.1029/2006GL025948.

Jacob, J., Y. Huang, J.-R. Disnar, A. Sifeddine, M. Boussafir, A. L. Spadano, and B. Turcq (2007), Paleohydrological changes during the last deglaciation in northern Brazil, *Quat. Sci. Rev.*, *26*, 1004–1015, doi:10.1016/j.quascirev.2006.12.004.

Kaiser, J., F. Lamy, and D. Hebbeln (2005), A 70-kyr sea surface temperature record off southern Chile (Ocean Drilling Program Site 1233), *Paleoceanography*, *20*, PA4009, doi:10.1029/2005PA001146.

Kessler, W. S. (2006), The circulation of the eastern tropical Pacific: A review, *Prog. Oceanogr.*, *69*, 181–217, doi:10.1016/j.pocean.2006.03.009.

Killops, S. D., and N. L. Frewin (1994), Triterpenoid diagenesis and cuticular preservation, *Org. Geochem.*, *21*, 1193–1209, doi:10.1016/0146-6380(94)90163-5.

Kim, J.-H., L. Dupont, H. Behling, and G. J. M. Verteegh (2005), Impacts of rapid sea-level rise on mangrove deposit erosion: Application of taraxerol and *Rhizophora* records, *J. Quat. Sci.*, *20*, 221–225, doi:10.1002/jqs.904.

Klein, S. A., and D. L. Hartmann (1993), The seasonal cycle of low stratiform clouds, *J. Clim.*, *6*, 1587–1606, doi:10.1175/1520-0442(1993)006<1587:TSCOLS>2.0.CO;2.

Klinkhammer, G. P., A. C. Mix, and B. A. Haley (2009), Increased dissolved terrestrial input to the coastal ocean during the last deglaciation, *Geochem. Geophys. Geosyst.*, *10*, Q03009, doi:10.1029/2008GC002219.

Kohfeld, K. E., and S. P. Harrison (2001), DIRTMAP: The geological record of dust, *Earth Sci. Rev.*, *54*, 81–114, doi:10.1016/S0012-8252(01)00042-3.

Koutavas, A., and J. Lynch-Stieglitz (2003), Glacial-interglacial dynamics of the eastern equatorial Pacific cold tongue-Intertropical Convergence Zone system reconstructed from oxygen isotope records, *Paleoceanography*, *18*(4), 1089, doi:10.1029/2003PA000894.

Koutavas, A., and J. P. Sachs (2008), Northern timing of deglaciation in the eastern equatorial Pacific from alkenone paleothermometry, *Paleoceanography*, *23*, PA4205, doi:10.1029/2008PA001593.

Koutavas, A., J. Lynch-Stieglitz, T. M. Marchitto, and J. Sachs (2002), El Niño-like pattern in Ice Age tropical Pacific sea surface temperature, *Science*, *297*, 226–230, doi:10.1126/science.1072376.

Lea, D. W., D. K. Pak, and H. J. Spero (2000), Climate impact of late Quaternary equatorial Pacific sea surface temperature variations, *Science*, *289*, 1719–1724, doi:10.1126/science.289.5485.1719.

Lea, D. W., D. K. Pak, C. L. Belanger, H. J. Spero, M. A. Hall, and N. J. Shackleton (2006), Paleoclimate history of Galápagos surface waters over the last 135,000 yr, *Quat. Sci. Rev.*, *25*, 1152–1167, doi:10.1016/j.quascirev.2005.11.010.

Leduc, G., L. Vidal, K. Tachikawa, F. Rostek, C. Sonzogni, L. Beaufort, and E. Bard (2007), Moisture transport across Central America as a positive feedback on abrupt climatic changes, *Nature*, *445*, 908–911, doi:10.1038/nature05578.

Leduc, G., L. Vidal, O. Cartapanis, and E. Bard (2009), Modes of eastern equatorial Pacific thermocline variability: Implications for ENSO dynamics over the last glacial period, *Paleoceanography*, *24*, PA3202, doi:10.1029/2008PA001701.

Leduc, G., R. Schneider, J.-H. Kim, and G. Lohmann (2010), Holocene and Eemian sea surface temperature trends as revealed by alkenone and Mg/Ca paleothermometry, *Quat. Sci. Rev.*, *29*, 989–1004, doi:10.1016/j.quascirev.2010.01.004.

Lisiecki, L. E., and M. E. Raymo (2005), A Pliocene-Pleistocene stack of 57 globally distributed benthic $\delta^{18}O$ records, *Paleoceanography*, *20*, PA1003, doi:10.1029/2004PA001071.

Liu, Z., and T. D. Herbert (2004), High-latitude influence on the eastern equatorial Pacific climate in the early Pleistocene epoch, *Nature*, *427*, 720–723, doi:10.1038/nature02338.

Lukas, R. (1986), The termination of the Equatorial Undercurrent in the eastern Pacific, *Prog. Oceanogr.*, *16*, 63–90, doi:10.1016/0079-6611(86)90007-8.

Lyle, M., N. Mitchell, N. Pisias, A. Mix, J. I. Martínez, and A. Paytan (2005), Do geochemical estimates of sediment focusing pass the sediment test in the equatorial Pacific?, *Paleoceanography*, *20*, PA1005, doi:10.1029/2004PA001019.

Mahowald, N., K. Kohfeld, M. Hansson, Y. Balkanski, S. P. Harrison, I. C. Prentice, M. Schulz, and H. Rodhe (1999), Dust sources and deposition during the Last Glacial Maximum and current climate: A comparison of model results with paleodata from ice cores and marine sediments, *J. Geophys. Res.*, *104*, 15,895–15,916, doi:10.1029/1999JD900084.

MARGO Project Members (2009), Constraints on the magnitude and patterns of ocean cooling at the Last Glacial Maximum, *Nat. Geosci.*, *2*, 127–132, doi:10.1038/ngeo411.

Markgraf, V., and H. F. Diaz (2000), The past ENSO record: A synthesis, in *El Niño and the Southern Oscillation Multiscale Variability and Global and Regional Impacts*, edited by H. F. Diaz and V. Markgraf, pp. 465–488, Cambridge Univ. Press, New York.

Martínez, I., L. Keigwin, T. T. Barrows, Y. Yokoyama, and J. Southon (2003), La Niña-like conditions in the eastern equatorial Pacific and a stronger Choco Jet in the northern Andes during the last glaciation, *Paleoceanography*, *18*(2), 1033, doi:10.1029/2002PA000877.

Martínez, I., D. Rincon, Y. Yokoyama, and T. Barrows (2006), Foraminifera and coccolithophorid assemblage change in the Panama Basin during the last deglaciation: Response to sea-surface productivity induced by a transient climate change, *Palaeogeogr. Palaeoclimatol. Palaeoecol.*, *234*, 114–126, doi:10.1016/j.palaeo.2005.10.022.

Martinez, J. I., and G. Bedoya (2001), Recent planktonic foraminifera from deep-sea sediments from the eastern equatorial Pacific: Proxies of the equatorial front in the late Quaternary, *J. Mar. Coastal Res.*, *30*, 151–176.

McGee, D., F. Marcantonio, and J. Lynch-Stieglitz (2007), Deglacial changes in dust flux in the eastern equatorial Pacific, *Earth Planet. Sci. Lett.*, *257*, 215–230, doi:10.1016/j.epsl.2007.02.033.

McPhaden, M. J., S. E. Zebiak, and M. H. Glantz (2006), ENSO as an integrating concept in Earth science, *Science*, *314*, 1740–1745, doi:10.1126/science.1132588.

Mechoso, C. R., et al. (1995), The seasonal cycle over the tropical Pacific in coupled ocean-atmosphere general circulation models, *Mon. Weather Rev.*, *123*, 2825–2838, doi:10.1175/1520-0493(1995)123<2825:TSCOTT>2.0.CO;2.

Medina-Elizalde, M., and D. W. Lea (2005), The mid-Pleistocene transition in the tropical Pacific, *Science*, *310*, 1009–1012, doi:10.1126/science.1115933.

Mix, A. C. (2006), Running hot and cold in the eastern equatorial Pacific, *Quat. Sci. Rev.*, *25*, 1147–1149, doi:10.1016/j.quascirev.2006.03.008.

Müller, P. J., and R. Schneider (1993), An automated leaching method for the determination of opal in sediments and particulate matter, *Deep Sea Res., Part I*, *40*(3), 425–444, doi:10.1016/0967-0637(93)90140-X.

Müller, P. J., G. Kirst, G. Ruhland, I. von Storch, and A. Rosell-Melé (1998), Calibration of the alkenone paleotemperature index $U^{K'}_{37}$ based on core-tops from the eastern South Atlantic and the global ocean (60°N–60°S), *Geochim. Cosmochim. Acta*, *62*(10), 1757–1772, doi:10.1016/S0016-7037(98)00097-0.

Neill, D. A. (1999), Vegetation, in *Catalogue of the Vascular Plants of Ecuador*, *Monogr. Syst. Bot.*, vol. 75, edited by P. M. Jørgensen and S. León-Yánez, pp. 8–13, Mo. Bot. Garden, St. Louis.

Neill, D. A., and P. M. Jørgensen (1999), Climates, in *Catalogue of the Vascular Plants of Ecuador*, *Monogr. Syst. Bot.*, vol. 75, edited by P. M. Jørgensen and S. León-Yánez, pp. 13–25, Mo. Bot. Garden, St. Louis.

Pahnke, K., J. P. Sachs, L. Keigwin, A. Timmermann, and S.-P. Xie (2007), Eastern tropical Pacific hydrologic changes during the past 27,000 years from D/H ratios in alkenones, *Paleoceanography*, *22*, PA4214, doi:10.1029/2007PA001468.

Paillard, D., L. Labeyrie, and P. Yiou (1996), Macintosh program performs time-series analysis, *Eos Trans. AGU*, *77*(39), 379, doi:10.1029/96EO00259.

Pailler, D., and E. Bard (2002), High frequency paleoceanographic changes during the past 140 000 yr recorded by the organic matter in sediments of the Iberian margin, *Palaeogeogr. Palaeoclimatol. Palaeoecol.*, *181*, 431–452, doi:10.1016/S0031-0182(01)00444-8.

Pak, H., and J. R. V. Zaneveld (1974), Equatorial front in the eastern Pacific Ocean, *J. Phys. Oceanogr.*, *4*, 570–578, doi:10.1175/1520-0485(1974)004<0570:EFITEP>2.0.CO;2.

Pena, L. D., I. Cacho, P. Ferretti, and M. A. Hall (2008), El Niño-Southern Oscillation-like variability during glacial terminations and interlatitudinal teleconnections, *Paleoceanography*, *23*, PA3101, doi:10.1029/2008PA001620.

Pennington, J. T., K.-L. Mahoney, V. S. Kuwahare, D. D. Kolber, R. Calienes, and F. P. Chavez (2006), Primary production in the eastern tropical Pacific: A review, *Prog. Oceanogr.*, *69*, 285–317, doi:10.1016/j.pocean.2006.03.012.

Peterson, T. C., and S. V. Russell (1997), An overview of the Global Historical Climatology Network temperature data base, *Bull. Am. Meteorol. Soc.*, *78*, 2837–2849, doi:10.1175/1520-0477(1997)078<2837:AOOTGH>2.0.CO;2.

Philander, S. G. H., D. Gu, D. Halpern, G. Lambert, N. C. Lau, T. Li, and R. C. Pacanowski (1996), Why the ITCZ is mostly north of the equator,

J. Clim., *9*, 2958–2972, doi:10.1175/1520-0442(1996)009<2958:WTIIMN>2.0.CO;2.

Pisias, N. G., and A. Mix (1997), Spatial and temporal oceanographic variability of the eastern equatorial Pacific during the late Pleistocene: Evidence from radiolaria microfossils, *Paleoceanography*, *12*, 381–393, doi:10.1029/97PA00583.

Poveda, G., P. R. Waylen, and R. S. Pulwarty (2006), Annual and inter-annual variability of the present climate in northern South America and southern Mesoamerica, *Palaeogeogr. Palaeoclimatol. Palaeoecol.*, *234*, 3–27, doi:10.1016/j.palaeo.2005.10.031.

Prahl, F. G., and S. G. Wakeham (1987), Calibration of unsaturation patterns in long-chain ketone compositions for paleotemperature assessment, *Nature*, *330*, 367–369, doi:10.1038/330367a0.

Prahl, F. G., T. Herbert, S. C. Brassell, N. Ohkouchi, M. Pagani, D. Repeta, A. Rosell-Melé, and E. Sikes (2000), Status of alkenone paleothermometer calibration: Report from Working Group 3, *Geochem. Geophys. Geosyst.*, *1*(11), 1034, doi:10.1029/2000GC000058.

Prahl, F. G., A. C. Mix, and M. A. Sparrow (2006), Alkenone paleothermometry: Biological lessons from marine sediment records off western South America, *Geochim. Cosmochim. Acta*, *70*, 101–117, doi:10.1016/j.gca.2005.08.023.

Raymond, D. J., S. K. Esbensen, C. Paulson, M. Gregg, C. S. Bretherton, W. A. Petersen, R. Cifelli, L. K. Shay, C. Ohlmann, and P. Zudeima (2004), EPIC2001 and the coupled ocean-atmosphere system of the tropical east Pacific, *Bull. Am. Meteorol. Soc.*, *85*, 1341–1354, doi:10.1175/BAMS-85-9-1341.

Richter, T. O., S. van der Gaast, B. Koster, A. Vaars, R. Gieles, H. C. de Stigter, H. de Haas, and T. C. E. van Weering (2006), The Avaatech XRF Core Scanner: Technical description and applications to NE Atlantic sediments, in *New Techniques in Sediment Core Analysis*, edited by R. G. Rothwell, *Geol. Soc. Spec. Publ.*, *267*, 39–50.

Rossel, F., E. Cadier, and G. Gómez (1996), Las inundaciones en la zona costera Ecuatoriana: Causas, obras de proteccion existentes y previstas, *Bull. Inst. Fr. Etud. Andines*, *25*(3), 399–420.

Rull, V. (1996), Late Pleistocene and Holocene climates of Venezuela, *Quat. Int.*, *31*, 85–94, doi:10.1016/1040-6182(95)00024-D.

Sachs, J. P. (2008), Divergent trends in Holocene SSTs derived from alkenones and Mg/Ca in the equatorial Pacific, *Eos Trans. AGU*, *89*(53), Fall Meet Suppl., Abstract PP23C-1486.

Sachs, J. P., R. R. Schneider, T. I. Eglinton, K. H. Freeman, G. Ganssen, J. F. McManus, and D. W. Oppo (2000), Alkenones as paleoceanographic proxies, *Geochem. Geophys. Geosyst.*, *1*(11), 1035, doi:10.1029/2000GC000059.

Schneider, R., P. J. Müller, and R. Acheson (1999), Atlantic alkenone sea surface temperature records, in *Reconstructing Ocean History: A Window Into the Future*, edited by I. Abrantes and A. C. Mix, pp. 33–55, Plenum, New York.

Shipboard Scientific Party (2003), Site 1239, *Proc. Ocean Drill Program Initial Rep.*, *202*, 1–93, doi:10.2973/odp.proc.ir.202.110.2003.

Sonzogni, C., E. Bard, F. Rostek, D. Dollfus, A. Rosell-Melé, and G. Eglington (1997), Temperature and salinity effects on alkenone ratios measured in surface sediments from the Indian Ocean, *Quat. Res.*, *47*, 344–355, doi:10.1006/qres.1997.1885.

Spero, H. J., K. M. Mielke, E. M. Kalve, D. W. Lea, and D. K. Pak (2003), Multispecies approach to reconstructing eastern equatorial Pacific thermocline hydrography during the past 360 kyr, *Paleoceanography*, *18*(1), 1022, doi:10.1029/2002PA000814.

Takahashi, K., and D. S. Battisti (2007), Processes controlling the mean tropical Pacific precipitation pattern: I. The Andes and the eastern Pacific ITCZ, *J. Clim.*, *20*, 3434–3451, doi:10.1175/JCLI4198.1.

Thompson, L. G., et al. (1998), A 25,000-year tropical climate history from Bolivian ice cores, *Science*, *282*, 1858–1864, doi:10.1126/science.282.5395.1858.

Tzedakis, P. C., D. Raynaud, J. F. McManus, A. Berger, V. Brovkin, and T. Kiefer (2009), Interglacial diversity, *Nat. Geosci.*, *2*, 751–755, doi:10.1038/ngeo660.

Versteegh, G. J. M., E. Schefuβ, L. Dupont, F. Marret, J. S. Sinninghe Damsté, and J. H. F. Jansen (2004), Taraxerol and *Rhizophora* pollen as proxies for tracking past mangrove ecosystems, *Geochim. Cosmochim. Acta*, *68*, 411–422, doi:10.1016/S0016-7037(03)00456-3.

Wang, C., and P. C. Fiedler (2006), ENSO variability and the eastern tropical Pacific: A review, *Prog. Oceanogr.*, *69*, 239–266, doi:10.1016/j.pocean.2006.03.004.

Wang, W., S. Saha, H.-L. Pan, S. Nadiga, and G. White (2005), Simulation of ENSO in the new NCEP coupled forecast system model (CFS03), *Mon. Weather Rev.*, *133*, 1574–1593, doi:10.1175/MWR2936.1.

Wang, X., A. S. Auler, R. L. Edwards, H. Cheng, P. Cristalli, P. L. Smart, D. A. Richards, and C.-C. Shen (2004), Wet periods in northeastern Brazil over the past 210 kyr linked to distant climate anomalies, *Nature*, *432*, 740–743, doi:10.1038/nature03067.

Waylen, P., and G. Poveda (2002), El Niño-Southern Oscillation and aspects of western South American hydro-climatology, *Hydrol. Processes*, *16*, 1247–1260, doi:10.1002/hyp.1060.

Weltje, G.-J., and R. Tjallingii (2008), Calibration of XRF core scanning for quantitative geochemical logging of sediment cores: Theory and application, *Earth Planet. Sci. Lett.*, *274*, 423–438, doi:10.1016/j.epsl.2008.07.054.

Winckler, G., R. F. Anderson, M. Q. Fleisher, D. McGee, and N. Mahowald (2008), Covariant glacial-interglacial dust fluxes in the equatorial Pacific and Antarctica, *Science*, *320*, 93–96, doi:10.1126/science.1150595.

Wittenberg, A. T., A. Rosati, N.-C. Lau, and J. J. Ploshay (2006), GFDL's CM2 global coupled climate models. Part III: Tropical Pacific climate and ENSO, *J. Clim.*, *19*, 698–722, doi:10.1175/JCLI3631.1.

Xie, S. P. (2004), The shape of continents, air-sea interaction, and the rising branch of the Hadley circulation, in *The Hadley Circulation: Present, Past and Future*, *Adv. Global Change Res.*, vol. 21, edited by H. R. Díaz and R. S. Bradley, pp. 121–152, doi:10.1007/978-1-4020-2944-8_4, Kluwer Acad., Dordrecht, Netherlands.

Xie, S. P., and S. G. H. Philander (1994), A coupled ocean-atmosphere model of relevance to the ITCZ in the eastern Pacific, *Tellus, Ser. A*, *46*, 340–350, doi:10.1034/j.1600-0870.1994.t01-1-00001.x.

Yeh, S. W., J. S. Kug, B. Dewitte, M. H. Kwon, B. P. Kirtman, and F. F. Jin (2009), El Niño in a changing climate, *Nature*, *461*, 511–514, doi:10.1038/nature08316.

Yin, J. H., and D. A. Battisti (2001), The importance of tropical sea surface temperature patterns in simulations of Last Glacial Maximum climate, *J. Clim.*, *14*, 565–581, doi:10.1175/1520-0442(2001)014<0565:TIOTSS>2.0.CO;2.

E. Bard, CEREGE, Aix-Marseille Université, CNRS, Collège de France, IRD, Europôle Méditerranéen de L'Arbois, BP 80, F-13545 Aix-en-Provence CEDEX 4, France.

T. Blanz and G. Leduc, Institut für Geowissenschaften, Christian Albrecht Universität, D-24118 Kiel, Germany.

S. Contreras, Max Planck Institute for Marine Microbiology, Celsiusstrasse 1, D-28359 Bremen, Germany.

F. Lamy, A. Mackensen, D. Rincón-Martínez, C. Saukel, and R. Tiedemann, Alfred Wegener Institute for Polar and Marine Research, Columbusstrasse, D-27568 Bremerhaven, Germany. (daniel.rincon.martinez@awi.de)